The Astrophysical Journal, 907:90 (13pp), 2021 February 1 https://doi.org/10.3847/1538-4357/abc475

Quality Metric for Spitzer–Braginskii and Grad 8 Moment Heat Flux Closures

J. D. Scudder
Department of Physics and Astronomy, University of Iowa, Iowa City, IA 52242, USA
Received 2020 July 23; revised 2020 October 18; accepted 2020 October 19; published 2021 February 1

Abstract

Quality metrics for Spitzer–Härm and Grad closures are presented based on the percentage of the heat flux moment supported only by nonnegative, physical, phase space densities $\mathbb{F} > 0$ underlying the closure. The Spitzer and Grad qualities exceed 95% for the perturbative regimes where Spitzer's formulation is analytically known to be convergent. Beyond this regime both heat flux qualities fall about 30% per decade increase of $\epsilon > 0.01$. In the solar corona the first decade's decrease in quality straddles the radius of the coronal temperature maximum and spans the initial acceleration of the solar wind. By the end of the second decade of increase of ϵ the observer is between 5 and $10R_{\odot}$, already in conditions comparable to those at 1 au with $\simeq$60% degradation of quality. These strong radial decays of closure quality show that integrating the fluid equations using such closures must represent a very poor assay of the role and effects of $\nabla \cdot \mathbf{q}$ had the heat flux been described throughout with a uniformly high quality closure procedure. For small ϵ, $\mathbb{F} < 0$ occurs for cosine of pitch angle $\mu < 0$ opposed to $\mathbf{q}$ at speeds above 2 thermal speeds and are omnipresent (but ignorable) for truly perturbative closures. Above a computed threshold in ϵ unphysical $\mathbb{F} < 0$ occurs for speeds below 2 thermal speeds with $\mu > 0$. The present work graphically shows $\mathbb{F} < 0$ regimes becoming increasingly pervasive as ϵ increases, first crossing $\simeq$4 thermal speeds at $\mu < 0$ and then representing ever larger unphysical incursions within the needed velocity sphere required to accurately determine the heat flux.

Unified Astronomy Thesaurus concepts: Astronomical models (86); Astrophysical fluid dynamics (101); Hydrodynamical simulations (767); Main sequence stars (1000); Plasma physics (2089); Solar coronal heating (1989); Solar corona (1483); Solar wind (1534); Stellar winds (1636)

1. Introduction

The drive for economy of description of astrophysical plasmas strongly encourages modelers to use a fluid model for these ionized gases. An essential part of such a model is its adopted closure that involves assumptions that allow a finite number of partial differential equations to approximate the much more difficult solution of the fully kinetic integro-partial differential Boltzmann equation. Using the chosen closure allows the solutions of a reduced set of equations to be analyzed to demonstrate consistency with the closure's assumptions while suggesting what heat would flow, how viscous stresses would be released, what frictions would be relaxed, and more generally how these plasmas might rearrange their profiles in response to the spatial gradients they are allowed to support. There is a wide range of strategies for arriving at fluid level descriptions and evaluating the assumptions that underlie these closure strategies.

While this paper focuses on a commonly used fluid approach for space plasma modeling, it does not tacitly argue for or against the relevance of other fluid models. At the paper's end a brief survey of closure approaches are compared and the suitability of their closure assumptions for modeling the corona and solar wind is briefly inventoried, sorting their approaches by the lessons learned about the SBG closure studies of the main paper.

The near coronae and winds of stars originate in high density stellar atmospheres where collisions are common. This paper explains and displays an objective measure of the quality for two specific plasma fluid closures used for such a regime, which are usually referred to as Spitzer–Braginskii (SB; Spitzer & Härm 1953) and Grad's 8 moment (G; Grad 1949) methods. The truncations made possible by these closures are based on a perturbation expansion (given in Equations (4) and (5)) for the underlying velocity distribution function (VDF) that for these closures is only slightly removed from the local thermal dynamic equilibrium expected in the high density stellar atmospheres proper. This parameter regime is often loosely referred to as the collisional regime for plasma fluid closures. The closures' VDFs provide an assumed bridge between their approximate compatibility with a world view of scattering and its enabling property to form any and all moments needed to truncate the otherwise infinite set of fluid moment equations needed to fully emulate the kinetic equation.

The SBG closure approach presumes that the Knudsen number, $K \ll 1$, is a small perturbative parameter, where $K = \lambda_{\rm mfp}/L$ is the ratio of the mean free path for scattering, λ, and the spatial scale of the realized fluid's gradients, L. Unfortunately K varies strongly with stellar radius and the SB closure is known to be invalid for $K > 0.01$ (Gurevitch & Isotomin 1979; Gray & Kilkenny 1980; Schoub 1983; Scudder & Olbert 1983). This situation makes the SB closure inappropriate for almost all of the corona solar wind volume, despite its current common use across this relatively accessible astrophysical plasma. Calculations with stellar data suggest that above $r > 1.05R_{\star}$ all stars on the main sequence have Knudsen numbers in excess of the upper limit of $K = 0.01$ for the physical consistency of SB closure (Scudder & Karimabadi 2013).

The quality measure developed in this paper illustrates the degradation of the SBG closures as K increases. The derived decrease in the quality reflects the increased fraction of heat flux supported by unphysically negative probabilities in the VDF, which is the central leverage for the closure. Above $K = 0.01$ the decay of the SBG closure quality reflects the extensive negative and unphysical probabilities within the closure's VDF that reach very low speeds in thermal units.

The high speed powers in the heat flux moments accentuate the importance and locales where VDF < 0, producing counter-intuitive effects such as negative phase space densities at negative cosine of pitch angle μ values adding to the parallel heat flux along $\mu = 1$. The heat flux weighted quality of SBG of this paper recovers the $K = 0.01$ boundary below which SBG is analytically known to be valid.

This paper does not seek to rehabilitate the Spitzer–Braginskii or Grad (SBG) closures for finite K astrophysical plasmas. Rather, the objective is to visualize the unphysical situation openly being condoned when SBG closures are used for plasma systems that have $K > 0.01$.

In the low corona and acceleration zone of the solar wind, conclusions continue to be drawn that the observed solar wind cannot be explained by heat conduction alone (Killie et al. 2004; Cranmer et al. 2007; Usmanov & Goldstein 2006; van der Holst et al. 2010, 2014; Chandran et al. 2011; Manchester et al. 2012; Gombosi et al. 2018; Reville et al. 2018; Schiff 2020; Matsumoto 2021). These modelers have used the SB or Grad closures, sometimes including additional physical processes to improve agreement with observations. This line of argument is then extended further, seeking to establish the centrality of new effects of wave-particle heating as the required ingredients to explain the coronal temperature inversion and drive the wind. This cantilevered set of arguments is done while retaining the Knudsen number inappropriate SB closure as the truncation justification for the finite fluid moment equations in the finite K regimes being modeled.

This paper provides a quantitative and visual way to see the unphysical behavior condoned by using SBG closures beyond the very small Knudsen numbers where they are analytically known to be valid. It demonstrates that the assumed velocity probability distribution function that enabled the closure becomes pervasively and unphysically negative, causing the heat flux and other moments to be increasingly determined by domains of negative total velocity probability distributions. Using such a dramatically unphysical heat law for closure in finite K regimes vacates any meaningful information from comparing its profiles with observables. Using the same fluid closure with additional physical effects still remains unphysically closed, but mathematically done with a broken SBG framework.

Unless specifically singled out for contrast or comparison, properties of closures discussed in this paper refer to SBG and are not necessarily asserted to be the properties of all closures. A look at alternate closures from the vantage point of the diagnosis of the SBG closure failures complete the discussion section at the end of this paper.

2. Background

Chapman–Enskog fluid closures, like SB, suggest functional relationships between the highest retained and lower moments that are then inserted into the fluid description. These relationships are the configuration space residues of the velocity space functional form used for the closure's phase space density, $\mathbb{F}(\mathbf{v}, \mathbf{A}, \epsilon)$, whose details are lost when forming the fluid moment equations. For the description of steady-state transport the values of A_i are chosen for certain conservation law purposes (e.g., quasi-neutrality, zero current parallel to $\hat{\mathbf{b}}$); ϵ is an identified dimensionless variable assumed to be small as the basis for linearizing the Boltzmann equation. In the Chapman–Enskog closure ϵ is the local Knudsen number, $K = \lambda/L_r$, where the mean free path and the shortest (rth) scale length among the moments are denoted by λ and L_r, respectively. The chosen $\mathbb{F}(\boldsymbol{v}, \boldsymbol{A}, \epsilon)$ is an approximate solution of the Boltzmann equation if ϵ is suitably small; for SBG closure these perturbations are developed as corrections to a local Maxwellian, e.g., Hazeltine & Waelbroeck (1998). As is well known, solutions of the Boltzmann equation with nonnegative initial conditions remain nonnegative everywhere in $\mathbf{x}$, $\mathbf{v}$, and t, consistent with their interpretation as probabilities.

The closure represents an assumption, whose consequences allow a fluid description dependent on $\mathbf{x}$ and t, but independent of $\mathbf{v}$ space properties. Such a fluid description appears to have no contact with the evolution of the plasma in velocity space. This appearance ignores the chain of approximations required to make the fluid equations a closed set of partial differential equations relating velocity space moments of the underlying distribution functions and their gradients, without monitoring the evolution of the probability distribution function $f(\mathbf{x}, \mathbf{v}, t)$.

This compartmentalization, while desired for the computational solution, gives the incorrect impression that these closed fluid equations are equally valid regardless of the solution profile properties that they produce. As is well known the solutions produced can easily violate the assumptions that allowed the mathematics of the closure to be formulated; the quality of the solution and the relevance of the closure minimally requires a posteriori checking that its assumptions are not contradicted by the solution. For example, if $K \ll < 1$ is assumed in the derivation $K(\mathbf{x})$ may not remain small across the domain of the solution, invalidating that solution profile.

A common form for the SBG closures for $\mathbb{F}$ has the form

$$\mathbb{F}(\boldsymbol{x}, \boldsymbol{v}, A, \epsilon, \epsilon) \simeq \frac{n(\boldsymbol{x})}{\pi^{3/2} w(\boldsymbol{x})^3} f_o(\nu)(1 - \epsilon(\boldsymbol{x})\mathbb{P}(\nu)\mu), \quad (1)$$

where f_o is an isotropic Gaussian, $\mathbb{P}$ is a polynomial in dimensionless speed $\nu = v/w(\mathbf{x})$, μ is the cosine of the traditional pitch angle, and $w(\mathbf{x})$ is the thermal speed spread of f_o. In the perturbative ϵ regime $\mathbb{F} > 0$ is implied almost everywhere by Equation (1). (Further details are shown below.) The spatial dependence of the presumed perturbative quantity $\epsilon(\mathbf{x})$ depends on the solutions that result from the closure. This variation is unknown until verified a posteriori; whether it remains uniformly and adequately small across the solution generated is the final justification of the perturbative assumptions. This inventory is only rarely performed and almost never discussed by the modelers of astrophysical plasmas that introduce SBG closures; a posteriori it is the only protection for the liabilities of the fluid modeler using SBG closures; otherwise there is no clear argument that the solution rests on a physical picture rather than a mathematical one.

For the popular Spitzer–Härm closure ϵ is the mean free path for scattering over the shortest background scale of gradients; not only do the fluid equations imply spatial variations in the mean free path, they also imply changes in the spatial scales of gradients of the solution also influenced by gravity, rotation, and radiation. The closure approach posits in advance that $\epsilon(\mathbf{x})$ remains perturbatively small through the spatial domain of the fluid solution that is fully capable of contradicting this assumption.

When used to derive steady-state spatial profiles SB closures choose $\mathbb{F}$ consistent with (i) zero steady-state currents parallel to $\hat{\mathbf{b}}$ and (ii) quasi-neutrality; only in this regime does this analysis produce a simple Fourier like heat law that only depends on the temperature and its gradients.

From observations in the solar wind and indirect indicators in other astrophysical plasmas, the $\epsilon = \mathcal{O}(1)$ regime is expected to be commonplace. For this regime Equation (1) predicts many places where $\mathbb{F} < 0$ and the perturbative closure approach is analytically known to be inconsistent. The present paper seeks to explore the idea that defective perturbation expansions have an accessible, physical thumb print: pervasive underlying negative velocity probability distributions $\mathbb{F} < 0$ used as proxies for local solutions to the Boltzmann equation.

The possibility of $\mathbb{F} < 0$ is not a new finding of this paper or for transport solutions. Often its occurrence is noted and discounted (especially when occurring at many thermal speeds) by appealing to the convergence produced by the Gaussian in Equation (1) for all moments needed to proceed with the closure algebra. Work has attempted to address these closure difficulties (Struchtrup 2005) and recent work (Ng et al. 2018) has illustrated attempts to sidestep this problem with Grad's closure by using a maximum entropy closure (Levermore 1996) that is at least guaranteed to be nonnegative.

The focus here is to ascertain how and when the negativity of $\mathbb{F}$ that attends a given adopted closure undercuts the quality of the moments determined using that closure, providing an objective basis for discounting interpretations of fluid solutions determined with these closures. Since Grad's approach to closure does not have an analytically known domain of validity this paper's technique allows an examination of Grad closure's VDF to see how its positivity and heat flux depend on its small parameter, which is the ratio of the heat flux to the so-called saturated heat flux. This approach gives a practical veto for accepting results with the Grad 8 moment closure as well.

Because Gaussians always dominate divergent polynomials, the moments of Equation (1) always exist. These converged numbers can easily be dominated by numerical contributions from the locales where $\mathbb{F} < 0$, even when this occurs where $|\mathbb{F}|$ is very small compared to the maximum of the Gaussian. Because the transport modified moment integrands go to zero at very high powers of speed (see the Appendix where exponents of 5, 8, 9,10, and 11 are involved), significant, if not dominant contributions to the moments can occur for speeds well removed from the Gaussian's peak (see Appendix Equation (26) for estimates). Thus the impact of $\mathbb{F} < 0$ can be significant on the heat flux moment, even when it occurs at speeds well above 3 thermal speeds when some might suggest they are of no concern. This will be made quantitative and visualizable below.

This paper exhibits as a function of ϵ the occurrence and systematics of what percentage of the local moment's value in the fluid equations is computed from velocity domains where $\mathbb{F}(\boldsymbol{v}, \boldsymbol{A}), \epsilon) < 0$ (Scudder 2019a). Specifically, if the Ith total reported moment is $\mathcal{M}^I$ and if $\mathcal{M}^I_-$ were the integrated contribution to the total moment from $\mathbb{F}(\mathbf{v}, \mathbf{A}, \epsilon) < 0$ locales, then the Ith quality, $\mathcal{Q}_I$, of the Ith moment is given by

$$\mathcal{Q}_I(\epsilon) = 100\frac{\mathcal{M}^I - \mathcal{M}^I_-}{\mathcal{M}^I} = 100\frac{\mathcal{M}^I_+}{\mathcal{M}^I}. \tag{2}$$

This quality quantifies the portion of the closure's prediction for the moment determined only by the physical part of the probability distribution function, $\mathbb{F} \geqslant 0$.

A moment of order I weights the underlying distribution function $\mathbb{F}$ with speed factors scaling $\propto v^{I+2}$. The higher the moment I value, the larger the weight's speed leverage to resist suppression by the unperturbed Gaussian factor in Equation (1). From this systematic the most stringent quality test for a closure comes from the highest moment I retained by the closed fluid equations. When closed at the energy equation, the desired quality test would be for the heat flux, III.

The size of the spatial variation of the quality factor across the fluid solution obtained also comments on the reliability of the heat flux source term used in the conservation equations, since they ideally would contain $\nabla \cdot \mathbf{q}_T$ with $\mathbf{q}_T$ being the physically accurate heat flux. When there is a degradation of quality the disparity between $\mathbf{q}_T$ and the value of $\mathbf{q}$ reported by a closure with quality $\mathbb{Q}$ has a relation of the form

$$\mathbf{q}_T = \mathbf{q} + \mathbb{R}(\mathbb{Q}(\mathbf{x})). \tag{3}$$

When $\mathbb{F} < 0$ occurs in a model such as Equation (1), the moment computations take on unphysical twists. As an example, ignoring that $\mathbb{F}$ should be nonnegative to be appropriate, one might argue that the ϵ correction term in Equation (1) makes no contribution to the density by orthonormality of Legendre polynomials. If one restricts one's attention to the part of the phase space where Equation (1) is nonnegative the surviving part of $\mathbb{F} \geqslant 0$ no longer enjoys this orthonormality. Confusing but true, the onset of $\mathbb{F} < 0$ is not necessarily attended by negative moments of density, trace of the pressure, or temperature. For the vector and tensorial moments the intrinsic algebraic cancellations that occur when the VDF > 0 are now complicated by new behavior that attends those phase space regimes where $\mathbb{F} < 0$.

This paper graphically shows that unphysical $\mathbb{F} < 0$ is present in these closures even when they are truly perturbative. These effects were ignorably small nuisances when $\epsilon \leqslant 0.01$ occurs. For finite ϵ their once ignorable unphysical negative probability distributions grow to envelope the phase space, dominating the fluid dynamic modeling in astrophysics, being terribly unfaithful to the Boltzmann equation they were supposed to approximate.

3. Two Perturbative Heat Flux Closures

The SBG perturbative closures have velocity probability distribution functions (Equations (4) and (5), below) that fit the simplified form of Equation (1). The physical meaning of the dimensionless ϵ in Equation (1) follows from the approximations of the perturbation expansion assumed. In CE and SB ϵ is determined by the pressure Knudsen number, $\mathbb{K}_P$, or the collisional mean free path over gradient scale; in Grad's 8 Moment closure $\epsilon(\mathbf{x})$ is assumed to be the dimensionless heat flux $\mathbb{QQ} = q_{\|}/q_{\rm sat}$, where $q_{\rm sat} \equiv 3nm_e w^3/4$, where $m_e w^2 \equiv 2kT_e$. These expansion factors are related, as shown in Equation (7).

The premise for closures of the type of Equation (1) is that the correction to unity remains small at all speeds and pitch angles. The polynomial in speed $\mathbb{P}$ is determined by the energy dependence of the collisions involved and the type of perturbation being attempted. Because $\mathbb{P}$ is analytic it eventually grows without bound, making it clear that whatever $\epsilon(x_o)$'s finite size, there will always be speeds v for the VDF in

x_o's locale for which the correction term in Equation (3) will exceed unity; together with odd parity of $\cos\theta$ this implies that the velocity distribution function VDF will become physically negative at that speed for some range of pitch angles.

3.1. Spitzer–Härm–Braginskii Closure

The Spitzer–Härm form of this type, f^S, is based on a Chapman–Enskog style expansion about a Maxwellian VDF associated with uniform parameters as presented, for example, by Hazeltine & Waelbroeck (1998):

$$\begin{aligned} f^S(\nu,\,\mu) &= f_o(\nu^2)[1 - \mathbb{K}_T\mathbb{P}^S(\nu)\mu] \\ f_o(\nu^2) &\equiv \frac{n}{\pi^{3/2}w^3}\exp(-\nu^2) \\ \mathbb{P}^S(\nu) &\equiv \frac{8}{27\sqrt{\pi}}\nu^4(4 - \nu^2), \\ \mathbb{P}^{*S} &= 1.5755 \\ \epsilon = \mathbb{K}_T &\equiv -\hat{\mathbf{b}}\cdot\nabla lnT\lambda_{\rm mfp}, \end{aligned} \tag{4}$$

where $\nu = v/w$ is the dimensionless speed measured in thermal speed units of f_o. The single speed maximum of $\mathbb{P}$ occurs at the indicated value $\mathbb{P}^{*S}$. In the correction to unity expression small terms have also been omitted that depend on the very small electron flow Mach number using the electron thermal speed. The derived form of Equation (4) with perturbations about a posited Maxwell–Boltzmann $f_o(v)$ shows that ϵ in this expansion about a uniform equilibrium is the temperature Knudsen number, $\mathbb{K}_T$.

3.2. Killie Version Grad's 8 Moment Method

The Grad form determines a modified 8-moment closure form given by Killie et al. (2004)

$$\begin{aligned} f^G(\nu,\,\mu) &= f_o(\nu^2)(1 - \mathbb{QQ}\cdot\mathbb{P}^G(\nu)\mu), \\ f_o(\nu^2) &\equiv \frac{n}{\pi^{3/2}w^3}\exp(-\nu^2) \\ \mathbb{P}^G &\equiv \frac{6\nu^3}{35}(7 - 2\nu^2) \\ \mathbb{P}^{*G} &= 1.46074 \\ \epsilon = \mathbb{QQ} &\equiv \frac{q_\parallel}{q_{\rm sat}}, \end{aligned} \tag{5}$$

where $q_{\rm sat} \equiv 3nkTw/2 = (3nmw^3)/4$. This form is a modification of the 8-moment closure suggested by Schunk (1977) and used to model the solar wind expansion. Recently this closure form was suggested to be better than Spitzer for coronal solar wind acceleration studies up to and beyond 1 au (Schiff 2020).

The functional forms in Equation (1) for f^G and f^S above will jointly be referred to as $\mathbb{F}$ below:

$$\mathbb{F}(\nu,\,\mu) \leftrightarrow \{f^G(\nu,\,\mu), f^S(\nu,\,\mu)\}. \tag{6}$$

Both were constructed to be mathematically consistent with zero parallel current, regardless of the size of ϵ or the occurrence of $\mathbb{F} < 0$; these integrated mathematical constraints were imposed on the function $\mathbb{F}$ without ensuring that $\mathbb{F}$ was physical throughout the integration domain of the velocity space.

Both Equations (4) and (5) possess heat flows scaling with the saturated heat flux parameter, $q_{\rm sat}$, given above:

$$\begin{aligned} q_\parallel &\equiv \frac{m_e w^6}{2}\int_0^\infty d^3\nu\mathbb{F}(\overline{\nu})\nu^3\mu \\ q_\parallel^{\,G} &\equiv \frac{3nmw^3}{4}\mathbb{QQ} = q_{\rm sat}\mathbb{QQ} \\ q_\parallel^{\,S} &\equiv = q_{\rm sat}\mathbb{K}_T. \end{aligned} \tag{7}$$

Unlike the Spitzer form the Grad value of $q_\parallel$ appears not to depend on gradients, but just the local value of density and temperature; to some extent this is illusory, since in that method there is another fluid evolution equation retained for $\mathbb{QQ}$, causing interdependence with all lower order moments and their gradients.

4. Inventory of Closure Quality

Recently Scudder (2019a) proposed to examine closure suitability by quantifying the impact of negative phase space densities on the moments used in the fluid equations that they support. This paper illustrates a mixed analytical and one-dimensional numerical integral formulation to assess the importance of $\mathbb{F} < 0$ in the moments for the SBG closures given above in Equations (4) and (5).

Assuming $\mathbb{F}$ is gyrotropic the fluid moments have the general form:

$$\mathcal{M}_I = 2\pi w^{I+3}\int_0^\infty d\nu\nu^2\int_{\mu=-1}^{\mu=1} d\mu\mathbb{F}(\nu,\,\mu)\mathcal{W}(\nu,\,\mu,\,I), \tag{8}$$

where $\mathcal{W}$ is the velocity space weight involved in the moment; as an example, the parallel heat flux is determined by the weight function $\mathcal{W}(\nu,\,\mu,\,III) = 0.5m_e\nu^3\mu$.

The suggested analysis is to investigate the size of $\mathcal{M}_{\pm,I}$ determined by

$$\mathcal{M}_{\pm,I} \equiv 2\pi w^{I+3}\int_0^\infty d\nu\nu^2\int_{\mu=-1}^{\mu=1} d\mu\mathbb{F}_\pm(\nu,\,\mu)\mathcal{W}(\nu,\,\mu,\,I), \tag{9}$$

where $\mathbb{F}_-(\nu,\,\mu)$ is only nonzero when $\mathbb{F}(\nu,\,\mu) < 0$; similarly $\mathbb{F}_+(\nu,\,\mu)$ is only nonzero when $\mathbb{F}(\nu,\,\mu) > 0$.

One measure of the failure of the closure is the percentage of the total reported moment supported by the unphysically negative $\mathbb{F}_-$ contribution (Scudder 2019a):

$$\mathcal{F}_I = 100\%\frac{\mathcal{M}_{I,-}}{\mathcal{M}_I} = 100\%\frac{\mathcal{M}_{I,-}}{\mathcal{M}_{I,-} + \mathcal{M}_{I,+}}, \tag{10}$$

that is the complement of the quality $\mathbb{Q}_I$ defined in Equation (3). Typically the quality metric of the closure will be strongly varying according to $\epsilon(\mathbf{x})$ across the modeled system. Examples of such common spatial decays of quality for both these closures are shown below (Figure 9) for an example of modeling the solar wind expansion.

Because the correction term to unity in Equation (1) is a completely separable function of ϵ, μ, and ν it is possible to find the limits on $\mu(\nu)$ algebraically, reducing the 3D moments to only a 1D integration over all ν. This implies that Equation (9) has an equivalent form involving only one

improper numerical integral form:

$$\mathcal{M}_{\pm,I} \equiv 2\pi w^{I+3} \int_0^\infty d\nu \nu^2 \int_{\mu(\pm,-,\nu)}^{\mu(\pm,+,\nu)} d\mu \mathbb{F}_\pm(\nu, \mu) \mathcal{W}(\nu, \mu), \tag{11}$$

where $\mu(-, \pm, \nu)$ are the extremes of μ for a given speed ν, where $\mathbb{F}_- \neq 0$ and where $\mu(+, \pm, \nu)$ are the extremes of μ for a given speed ν, where $\mathbb{F}_+ \neq 0$. If for a given speed ν_o no μ interval exists, the μ integrated contribution from the ν_o speed shell becomes zero by the convergence of the two μ limits of integration. All of the moments of initial interest are of this separable type.

An explicit example to be used below for the heat flux integral exploits this separability, reducing to a single improper integral form

$$\begin{aligned}
\mathcal{M}_{-,III} &\equiv \mathbb{A} \int_0^\infty d\nu \exp(-\nu^2)\nu^5 \left[\frac{\mu^2}{2} - \epsilon \mathbb{P}(\nu)\frac{\mu^3}{3}\right]\Bigg|_{\mu(-,-,\nu)}^{\mu(-,+,\nu)} \\
&\equiv \mathbb{A} \int_0^\infty d\nu \exp(-\nu^2)\nu^5 [\tau(\nu) - \epsilon\zeta(\nu)\mathbb{P}(\nu)] \\
\tau(\nu) &= \frac{1}{2}((\mu(-,+,\nu))^2 - (\mu(-,-,\nu))^2) \\
\zeta(\nu) &= \frac{1}{3}((\mu(-,+,\nu))^3 - (\mu(-,-,\nu))^3) \\
\mathbb{A} &\equiv \frac{n_e m_e w^3}{\sqrt{\pi}}.
\end{aligned} \tag{12}$$

The remaining work is to specify $\mu(-, \pm, \nu)$.

5. Numerical Improper Integral: $\nu_\int$

Because the moments integrals are improper, the troublesome issue of numerically performing Equation (12) requires either mapping the semi-infinite domain to a finite domain together with a Jacobian, or finding a sufficiently large finite upper limit, call it $\nu_\int$, so that little error accompanies the proper integral approximation:

$$\int_0^\infty g(\nu)d\nu \simeq \int_0^{\nu_\int} g(\nu)d\nu, \tag{13}$$

while performing a maximally dense sampling of the selected finite interval.

When moments of this type can be done analytically they involve $\Gamma(q)$, Euler's gamma function. A common method for numerically handling integrals of this type is discussed in the Appendix for the heat flux integral. There a lowest allowable size $\nu_\int \simeq 3.9$ is estimated. The numerical integrals of this paper are done for $0 \leqslant \nu \leqslant 6$ so that even the very small contributions above the 3σ contributions estimated in the Appendix are numerically retained in the results below.

Throughout the text below $\nu_\int$ will be an important reference boundary for judging when $\mathbb{F} < 0$ effects start to reduce the quality $\mathcal{Q}_{\rm III}$ of these heat flux closures. As an example it is shown that the regime of maximum convergence known for Spitzer–Härm is recovered by the present approach, essentially the ϵ regime where $\mathbb{F} < 0$ starts to encroach inside the sphere estimated by $\nu_\int \simeq 3.9$ (see Figure 3).

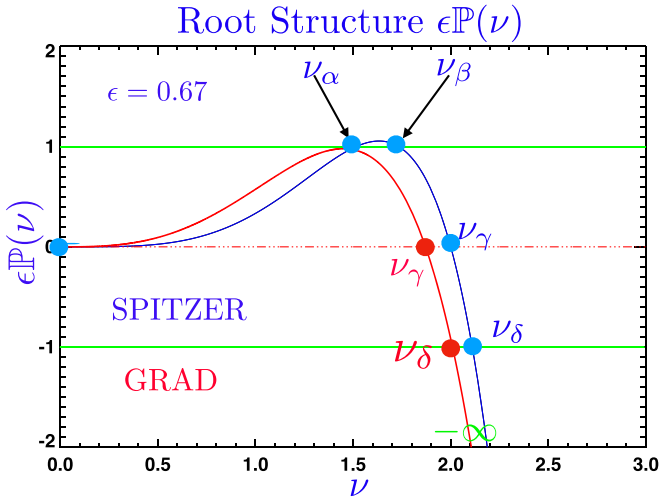

Figure 1. Profiles of $\epsilon\mathbb{P}(\nu)$ for Spitzer (blue) and Grad (red) closures for $\epsilon = 0.67$. (The maximum of the Grad curve is below unity.) The polynomials are bounded positively at small ν, between two speed zeros at $\nu = 0$ and $\nu \simeq 2$, but diverge toward negative infinity when $\nu \simeq 2$.

5.1. Making the Integrals Fast

The polynomial closure forms in Equation (1) depend on three-dimensionless variables: $\{\epsilon, \nu, \mu\}$. The generic structure of $\mathbb{P}$ for both Spitzer and Grad 8 moment closures is shown in Figure 1 and will be exploited to simplify the needed integrals to the 1D form of Equation (12).

5.2. Where is $\mathbb{F} < 0$?

Unphysical VDFs with $\mathbb{F} < 0$ are determined by the real, allowed roots for $\{\epsilon, \mu, \nu\}$ that simultaneously satisfy the two conditional inequalities:

$$\begin{aligned}
&1 - \epsilon\mathbb{P}(\nu)\mu < 0 \\
&-1 \leqslant \mu \leqslant 1.
\end{aligned} \tag{14}$$

For each ϵ there is a restricted problem in the $\{\mu, \nu\}$ variables to find regions that satisfy the first inequality in Equation (14). These boundaries can be found analytically, accelerating the exploration of this problem and its dependence on ϵ. By far the most complicated determinant in these bounds is the speed dependence of the polynomials $\mathbb{P}(\nu)$ surveyed next for their common properties. The $\{\mu, \nu\}$ regions where Equation (14) is satisfied provide the velocity space limits of integration needed to determine how much such regions contribute to the reported moments of the closure.

5.3. Structure of $\mathbb{P}$

The speed profiles for Spitzer and Grad closure $\mathbb{P}(\nu)$ from Equations (4) and (5) are indicated by blue and red curves, respectively, in Figure 1 for the given value of ϵ. Both curves are bounded positively at low speeds below ν_γ. Two speed zeros occur at $(0, \nu_\gamma)$ as indicated by filled dots with colors the same as the model's $\mathbb{P}$ curve. Importantly, both polynomials diverge for large speed toward $-\infty$; being bounded positively, these analytic functions must diverge with large negative values beyond $\nu > \nu_\delta > \nu_\gamma$.

The perturbation parameter ϵ linearly scales the magnitude of the heat flux, but also controls the complexity of the phase space volume where $\mathbb{F} < 0$ occurs. Speed roots of

$|\epsilon\mathbb{P}(\nu)| = 0, 1$ specify important changes in behavior, tagged by (4) filled cyan circles for Spitzer closure and (3) red ones for the Grad closure (one of the red circles is underneath a cyan one at the origin). With the size of ϵ chosen for this illustration there are no analogs for the Grad closure of the indicated ν_α or ν_β points for Spitzer's closure. They bound a ν interval where $\epsilon\mathbb{P}(\nu) \geqslant 1$. As shown for Spitzer's closure, when $\epsilon\mathbb{P} \geqslant 1$ the new locations for ν_α and ν_β will exist. When present the phase space becomes more complicated with an additional region (II below), where $\mathbb{F} < 0$.

$\mathbb{P}$: Since physical roots require $|\mu| \leqslant 1$, the conditions for roots for $\mathbb{F} < 0$ must be consistent with this additional inequality. An exhaustive set of possibilities on the size of $\epsilon\mathbb{P}$ yields the corresponding conditions for μ where non-physical $\mathbb{F} < 0$ will occur: Region I $\epsilon\mathbb{P} < -1$:

$$\begin{aligned}
&\text{If } 1 > \epsilon\mathbb{P}(\nu) > 0: \leftrightarrow\ 1 < \frac{1}{\epsilon\mathbb{P}(\nu)} < \mu = \varnothing \text{ (i)}\\
&\text{If } -1 < \epsilon\mathbb{P}(\nu) < 0: \leftrightarrow\ -1 > \frac{-1}{\epsilon|\mathbb{P}(\nu)|} > \mu = \varnothing \text{ (ii)}\\
&\text{If } \epsilon\mathbb{P}(\nu) < -1: \leftrightarrow\ -1 \leqslant \frac{-1}{\epsilon|\mathbb{P}(\nu)|} < \mu < 0 \text{ (iii)}\\
&\text{If } \epsilon\mathbb{P}(\nu) > 1: \leftrightarrow\ +1 \geqslant\ \mu > \frac{1}{\epsilon\mathbb{P}(\nu)} > 0 \text{ (iv).}
\end{aligned} \tag{15}$$

For $\mathbb{F} < 0$ contingencies (i, ii) have no solutions with $-1 \leqslant \mu \leqslant 1$, actually delimiting the opposite physical domains where $\mathbb{F} > 0$ at all physical pitch angles.

Conditions (iii) and (iv) in Equation (15) define two possible disjoint locales of $\mathbb{F} < 0$. Inequality (iv) presumes that $\epsilon\mathbb{P}^* > 1$ that for general ϵ may not occur (consider the Grad profile in Figure 1); this phase space domain's occurrence depends on a sufficiently large value of ϵ and controls Region II effects discussed below. By contrast, condition (iii) is generally possible for speeds $\nu > \nu_\delta$; this omnipresent domain of unphysical $\mathbb{F}$ is labeled Region I below. When Region II effects are present it represents a serious further degradation of the heat flow quality, $\mathcal{Q}_{\rm III}$, shown below.

5.4. Two Zones Where $\mathbb{F} < 0$

Conditions (iii) and (iv) in Equation (15) determine the conditions for two different phase space regions where $\mathbb{F} < 0$ can occur:

Region I: The Region I condition for $\mathbb{F} < 0$ reduces to the conditions:

$$-1 \leqslant \frac{-1}{\epsilon|\mathbb{P}(\nu)|} < \mu < 0; \quad \nu \geqslant \nu_\delta \tag{16}$$

that can always be satisfied for $\nu > \nu_\delta$, since by definition $\mathbb{P}(\nu_\delta) \equiv -1$ as shown in Figure 1. The smallest speed where this inequality is first met is ν_δ. While the existence of Region I with $\mathbb{F} < 0$ does not depend on the size of ϵ, the minimum value of the speed $\nu_\delta(\epsilon)$ where this region can occur does depend on ϵ. Geometrically this can be foreseen since increasing ϵ raises the maximum of $\epsilon\mathbb{P}$ while the polynomial must still go through the same zero at $\nu = \nu_\gamma$. Thus, increasing ϵ causes the $\epsilon\mathbb{P}$ curve to pass through zero more steeply at $\nu = \nu_\gamma$ and transiting -1 more immediately than for weaker ϵ, making $\nu_\delta(\epsilon)$ a decreasing function of increasing ϵ that will be explicitly shown below in Figure 3.

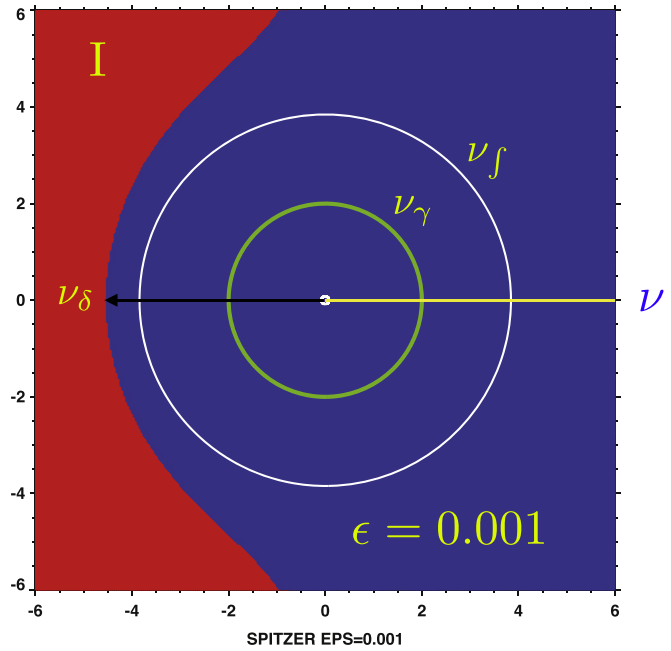

Figure 2. Illustration in red of Region I of phase space where perturbative $\epsilon = 0.001$ Spitzer closure distribution $\mathbb{F} < 0$ is shown as a function of pitch angle and dimensionless speed $\nu = v/w$; v is the particle speed and w is the thermal width of the reference Gaussian. The complementary blue part of phase space corresponds to $\mathbb{F} > 0$. The yellow horizontal axis is the $\mu = 1$ pole of this presentation in pitch angle format, while Cartesian speed distances in normalized units $\nu = v/w_e$ are indicated along the box's perimeter. ν_δ is the minimum speed radius of the red–blue interface in the figure, and corresponds to where $\epsilon\mathbb{P}(\nu_\delta) = -1$ in Figure 1 above.

An example of the sign partition of gyrotropic phase space determined by Equation (16) is shown in Figure 2 for a perturbatively small $\epsilon = 0.001$ for the Spitzer closure. (This regime is below the known upper limit for ϵ for the SB closure discussed above.)

The Region I boundary is at nonpositive $\mu \leqslant 0$, with the Region I part of phase space indicated in red and at speeds larger than the radius of this boundary at a given negative pitch angle. The green and white circles are concentric about the Gaussian rest frame origin, showing that the red–blue interface between Region I and the blue zone for physical $\mathbb{F} > 0$ flares outwards from $\mu = -1$ from a circular form about the origin. This implies that the pitch angle averaged speed of this red–blue boundary, $\overline{\nu_{\mu\leqslant 0}}$, exceeds the minimum speed on this boundary, ν_δ, that always occurs at pitch angle $\theta = \pi$, opposed to the yellow segment that denotes the pole of the pitch angle phase space.

The outer white circle at speed $\nu_\int$ is the minimum acceptable maximum speed upper limit when approximating the improper heat flux moment numerically (estimated in the Appendix); it is of considerable importance in this paper.

This picture shows that, for this value of ϵ, Region I domains of $\mathbb{F} < 0$ are present but do not penetrate within the spherical speed $\nu_\int$ necessary to obtain a convergent value for the heat flux integral. The contributions from blue regions where $\mathbb{F} > 0$ and inside the sphere of radius $\nu_\int$ are more than sufficient to determine the reported moment without any (significant) contributions from $\mathbb{F} < 0$. In these circumstances the cavalier

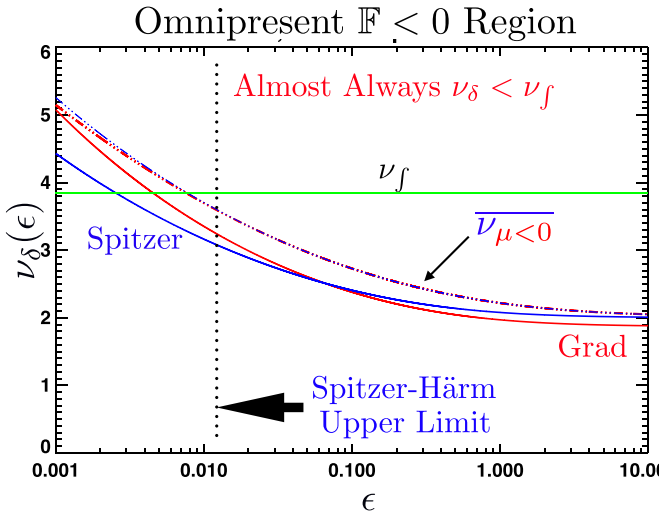

Figure 3. Minimum speed ν_δ for $\mathbb{F} < 0$ intrusion for $\mu < 0$, for Grad 8 Moment (red) and Spitzer (blue) closures. Dashed–dotted curves indicate variation of negative pitch angle averaged speed $\overline{\nu_{\mu<0}}$ of the intrusion boundary of $\mathbb{F} < 0$. While higher than ν_δ, both are generally below $\nu_\int$, with the pitch angle averaged speed crossing $\nu_\int$ at ϵ values nearly coincident with the known Spitzer–Härm limit of the perturbation expansion.

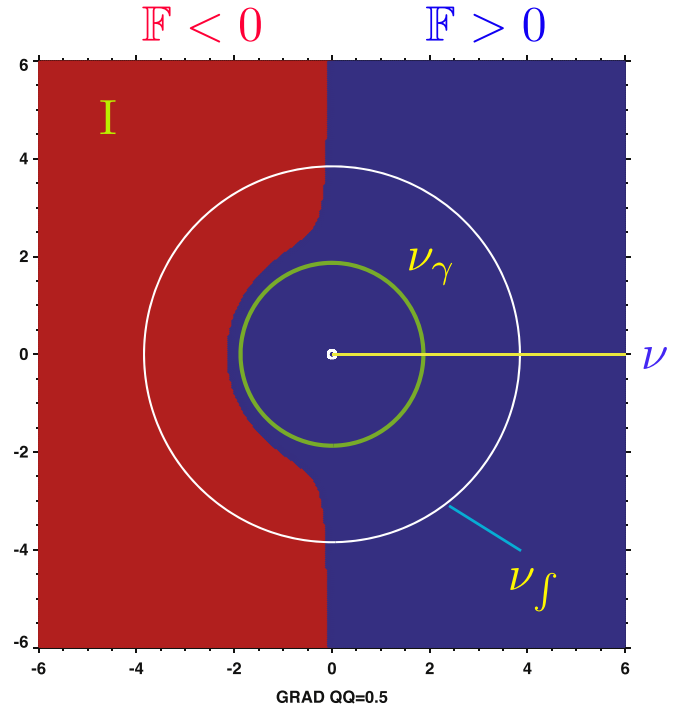

Figure 4. Pitch angle distribution for $\mathbb{F}(\overline{\nu})$ for Grad's closure with $\mathbb{QQ} = 0.5$. The blue region indicates where $\mathbb{F} > 0$, while red regions indicate unphysical domains where $\mathbb{F} < 0$. Green circle indicates ν_γ, where $\mathbb{P}$ has its largest speed zero. Larger white circle at $\nu_\int$ is the minimum–maximum radius in velocity space needed to get a reasonably accurate heat flux moment (see the Appendix). Small white circle is the minimum–minimum speed needed for the moment integration.

integration over the entire velocity space makes no difference to a more rigorous inventory of contributions only from $\mathbb{F} > 0$.

Throughout the remainder of the paper it will be shown that as ϵ grows, ν_δ decreases, and the Region I supports of the closure with $\mathbb{F} < 0$ intrude more and more inside the $\nu_\int$ sphere that determines the heat flux. This implies the closure's heat flow predictions are more and more reliant on unphysical distribution functions, implying increasingly poorer qualities $\mathcal{Q}_{\rm III}(\epsilon)$ as shown below in Figure 6.

The variation of $\nu_\delta(\epsilon)$ is shown with solid red and blue curves for both closures in Figure 3; they are generally below $\nu_\int$, the minimum–maximum speed shown in the Appendix required to estimate the heat flow moment numerically with precision. Of subsequent interest is the negative pitch angle averaged speed profiles $\overline{\nu_{\mu<0}}$ of the intrusion boundary of $\mathbb{F} < 0$, shown as red and blue dashed–dotted curves for the two transport models. Because of the flaring of the red–blue interface it is clear that $\overline{\nu_{\mu<0}} > \nu_\delta$ with the average boundary always exceeding the minimum ν_δ, being most disparate from it at very small ϵ.

The very small initial range in this figure where $\overline{\nu_{\mu<0}} > \nu_\int$ corresponds to the convergent range for Spitzer–Härm (below the vertical black dashed line at 0.01), where though present, $\mathbb{F} < 0$ is arguably ignorable in a quantitative sense for informing the moment of the closure. It should be recalled that this upper limit for Spitzer–Härm was determined by analysis of the convergence of perturbation expansions, a rather difficult subject for analysis and not always possible to be performed for new proposed closures. By contrast, the quality technique requires only that the closure function be specified for the positivity issues to be examined.

For $\epsilon > 0.01$, where it is known that Spitzer–Härm is inappropriate, the present approach (Figure 3) uniformly shows via $\overline{\nu_{\mu<0}} < \nu_\int$ and that $\mathbb{F} < 0$ is an increasing determinant of the closure moment. Interestingly, the analogous boundary for Grad's closure (red dashed–dotted curve) shows nearly identical behavior, suggesting that whatever promising aspects are perceived in Grad's closure formulation, it too is on as weak a foundation as Spitzer–Härm for $\epsilon > 0.01$, despite recent arguments to the contrary (Schiff 2020).

The blue dashed–dotted curve of $\overline{\nu_{\mu<0}}$ is consistent with restating the location of the known failure regime for Spitzer–Härm located at the vertical black dashed line. Grad's $\overline{\nu_{\mu<0}}$ curve in red is imperceptibly different from that determined for the Spitzer closure.

A similar presentation for larger $\epsilon = 0.5$ using Grad's closure is shown in Figure 4. The general (Region I) negative part of phase space is enlarged relative to the perturbative previous case, but still occurs only at nonpositive pitch angles. The minimum speed of intrusion is now well inside of $\nu_\int$ and approaching the green circle, corresponding to ν_γ in Figure 1. The red–blue interface is increasingly more circular. From this picture it is clear that there is a significant volume of $\mathbb{F} < 0$ that is within the domain that determines the value of the heat flux.

This figure demonstrates the important, asymmetric insurgence of negative $\mathbb{F} < 0$ (shaded red) within the radius $\nu_\int$ required to determine the heat flux for this value of ϵ. The blue domain of physical $\mathbb{F} > 0$ is also asymmetric as viewed in the rest frame of the lowest-order Maxwellian. It is unclear whether the imbalance of locales where $\mathbb{F} > 0$ will impact the quality of the heat flux predicted by such a model. These concerns are compounded by asymmetrical contributions from Region I that are also increasingly determining the heat flow. In general why should these biases not contribute further to the decreased quality for the theory to predict the size of the heat flow? The role of this asymmetric sampling in supporting the heat flux or skewness moment defined over all speeds and pitch angles is far from clear.

The preliminary indication is that the skewness about a Gaussian will be determined by the amplitude of the heat flux integral within the $\nu_\int$ sphere; as ϵ increases this shell is being increasingly distorted by contributions arising from unphysical $\mathbb{F} < 0$. Figures 2 and 4 only suggest part of the story of the importance of $\mathbb{F} < 0$ for the closure, since it does not take the full measure of the topography (ordinate) of the heat flux integrand, focusing at present on the biased sampling present of limits of physical versus unphysical $\mathbb{F}$ under all speed moments for this location.

When $\mathbb{F} < 0$ is considered one often hears arguments that the incidence of $\mathbb{F} < 0$ is not really important, since it occurs, as shown here, at speeds greater than 2 thermal widths ($\nu > 2$), away from the dominant Gaussian core of Equation (1). This paper is about the distinction of $\mathbb{F}$ being negative versus the integrated effect of that negativity on the quality of the closure's reported moment. As shown analytically below the structure of the heat flux integrand and all the moments deemphasize the vicinity of the velocity speed origin where the Gaussian dominates (see the Appendix); the contribution to the moments is determined by the competition between polynomial growth with increasing speed as against suppression by the Gaussian's exponential behavior. True, the suppression always wins eventually, making the moment convergent, but if $\mathbb{F} < 0$ occurs at critical places it can have a big impact on the integrated moment and the locations where this occurs are actually least effective if concentrated near the origin. In this sense the quality measure developed here seeks to evaluate that competition. (Insight to that competition is developed analytically in the Appendix.)

Region II: $\epsilon^*\mathbb{P} > 1$: As indicated above in Figure 1 from the profile of $\mathbb{P}$ something new is possible for $\mathbb{F} < 0$ when $\epsilon\mathbb{P} > 1$. This new behavior is reflected in a new Region II phase space volume where $\mathbb{F} < 0$ that corresponds to the occurrence of an island at positive pitch angles, where $\mathbb{F} < 0$ inside $\nu_\gamma \simeq 2$ shown in Figure 5. Since the polynomial functions in Equation (1) are fixed by the type of expansion and scattering assumed, the incidence of this phase space Region II island is contingent on the increased size of ϵ. Because of this geometrical threshold it implies that there are ranges of

$$\epsilon < 1/\mathbb{P}^*: \quad \max[\mathbb{P}] \equiv \mathbb{P}^*, \tag{17}$$

where the island will not occur. After passing this threshold in Equation (17), the unphysical island's speed shell width increases and its Region II pitch angle extent grows to almost, but not completely, fill the forward pitch angles inside of $\nu = \nu_\gamma$ indicated by the green ν_γ circle in the figure delineated by the joint inequalities:

$$\begin{aligned} &\nu_\alpha < \nu' < \nu_\beta \\ &1 > \mu \leqslant \frac{1}{\epsilon\mathbb{P}(\nu')} > 0. \end{aligned} \tag{18}$$

This relation shows that the island is bounded by the speeds of ν_α and ν_β, with pitch angles delimited by the second inequality in Equation (18).

The (i) larger Region I domain and (ii) smaller Region II speed island for $\mathbb{F}(\nu) < 0$, when present, occur with opposite pitch angles as shown in Figure 5. The total heat flux is expected to be positive along the yellow axis. The contributions δq to the heat flux from the two regions of $\mathbb{F} < 0$ involve

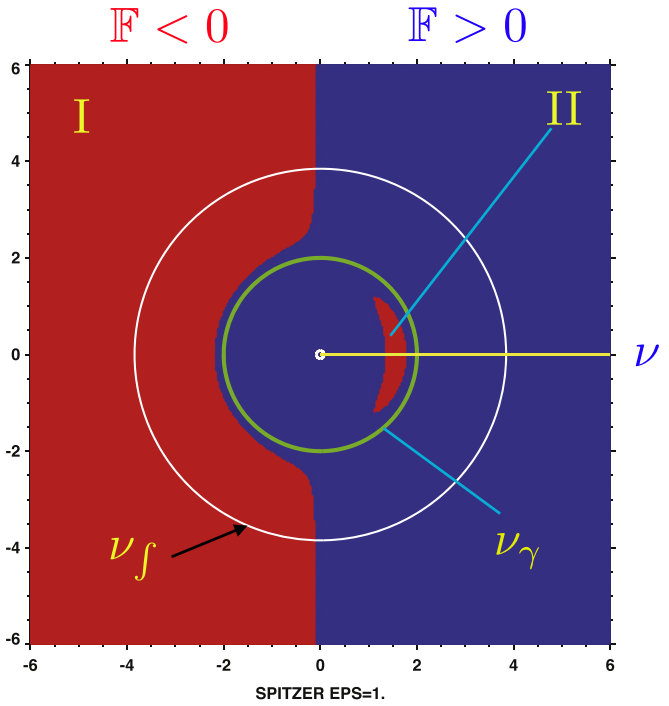

Figure 5. Same format as Figure 4, but here for $\epsilon\mathbb{P}^* > 1$ and $\epsilon = 1.0$. New phase space feature is the Region II island inside the green circle, where a zone of $\mathbb{F} < 0$ is possible that is disjoint from Region I. In this regime the general Region I of $\mathbb{F} < 0$ for speeds $\nu > \nu_\delta$ remains much as seen previously in Figure 4; because this is a larger perturbation the Region I boundary crowds the green circle more strongly than in Figure 4, while adding Region II's island effects.

products that are proportional to

$$\text{Sign}[\delta q] \propto (\mathbb{F} - 1)\nu^3\mu \propto (|a|_I - |b|_{II}), \tag{19}$$

which is positive for Region I contributions and negative for Region II locales. This algebra shows that heat flux is being assembled with increments contributing energy flux in opposite directions to the directions of the particles said to be producing the energy flow increments! Because the region I speeds exceed the region II domains, the net contribution is along the yellow pole of these figures. This odd behavior also occurs when only Region I $\mathbb{F} < 0$ locales occur. The Region I particles are all moving opposite to the direction of the yellow half ray, but this algebraic inventory insists that they add to the energy flux of heat along the yellow axis. These algebraic occurrences seem surreal, and although supporting increasing heat flows with increasing ϵ, have a very unphysical character.

The real problem arises because $\mathbb{F} < 0$ has been allowed to contribute to the moment. Contributions to the heat flux for particles supporting $\mathbb{F} < 0$ are unphysical and do not meet the basic positivity requirement for a Boltzmann equation probability density solution proxy.

When only Region I unphysical $\mathbb{F} < 0$ occur, excluding their contributions from the reported heat flux correctly infers the quality and level of support that the remaining positive $\mathbb{F} > 0$ contribute to the support of the moment. When Region II can occur, its corrections to the moment heat flux partially cancel those from Region I, understating the magnitude of the unphysical sensitivity of the moment. A partial response to this problem is to recompute $\mathcal{M}_-$ using the absolute value of their integrands using $|\mathbb{F} < 0|$ contributions. When this is done the

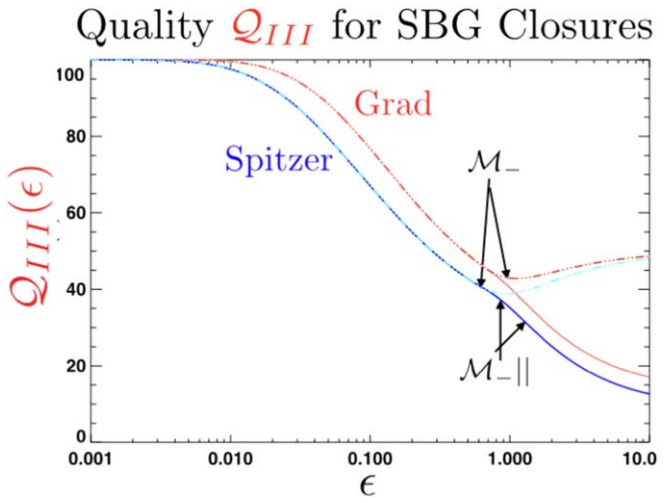

Figure 6. Spitzer and Grad variations of heat law quality, $\mathcal{Q}_{\rm III}(\epsilon)$ as a function of the size of ϵ. This quality measure for the heat flow is related to the FOM of Scudder (2019a) by the simple relation FOM $= 100\% - \mathcal{Q}_{\rm III}$.

quality figure for both models continues to fall with increasing ϵ and does not appear to level off as in Figure 6. When Region II is not present, these two methods give exactly the same result.

All of the $\mathbb{F} < 0$ behavior documented above has always been a part of all the moments made from these closures. Perhaps the fact that the integrals were done analytically in terms of gamma functions has obscured the unphysical character of those places (even in those integrands), where $\mathbb{F} < 0$. After the moment integrals are done in closed form and the closure relation is imposed as a condition between moments and their gradients, it becomes a veneer that hides potentially pervasive unphysical velocity space liabilities. However, just as discussed previously (Scudder 2019a) it does remain possible to inquire from the fluid solution whether its properties are consistent a posteriori with the assumptions made when deriving the closure. That is the full measure of the closure's quality for the problem at hand.

6. Sensitivity of $\mathcal{Q}_{\rm III}(\epsilon)$

An overview is now possible in Figure 6 of the systematic effects of increases in ϵ on the heat quality $\mathcal{Q}_{\rm III}(\epsilon)$ of the Spitzer and Grad closures in Equations (3) and (4). (i) The heat flow quality deteriorates with increasing ϵ. (ii) Typical astrophysical plasma systems have variations in ϵ that easily span the range of this figure, implying that the quality of closure varies widely with position in the same system. (iii) The canonical Spitzer–Härm convergent regime of $\epsilon \leqslant 0.01$ corresponds to $\mathcal{Q}_{\rm III} > 95\%$ in this presentation. (iv) Both Spitzer and Grad closures suffer losses of quality at the rate of the order of 30% per each decade increase of ϵ. (v) Region II $\mathbb{F} < 0$ effects cloud the picture beyond $\epsilon > 0.7$, but the quality of heat closure in this regime and higher is not much better than 30% founded on physical (nonnegative) velocity distributions. (vi) Attempting to model energetics across a system that spans such a range of ϵ has little likelihood of producing an actionable inventory of properties for comparison with observables. (vii) Neither Grad nor Spitzer are immune to this degradation of heat flow quality; this is not particularly surprising given the similar polynomial character of the proxy distribution functions. Considerable blame for these sensitivities must be associated with the choices that led to closures of the form in Equations (3) and (4).

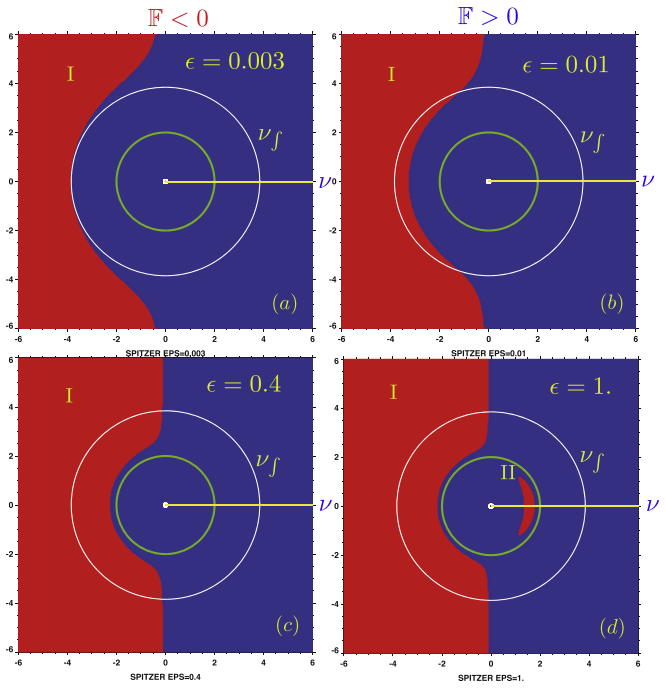

Figure 7. Spitzer progression of $\mathbb{F} < 0$ with increasing ϵ. The insets (a)–(d) have increasing values of ϵ in the set $\{0.003, 0.01, 0.4, 1.0\}$. The steady increase of incursions of Region I $\mathbb{F} < 0$ is clearly illustrated in the smaller ϵ examples; the onset of the disjoint Region II regime is shown in the $\epsilon = 1$ inset (d).

7. Spitzer Quality versus Analytical Estimates for Valid Closure

A graphical view of the progression in Figure 6 is shown in Figures 7 and 8. Four pitch angle portraits are organized for increasing ϵ for each closure model. The progressions are very similar, with slight differences because the order of the polynomials are different by one power. Insets (a) and (b) were chosen to illustrate the evolution of the first intrusion of Region I $\mathbb{F} < 0$ parts of the phase space across the sphere of speed $\nu = \nu_\int$ necessary to determine the heat flux. In inset (a) the heat flux moment can be determined without using the predictions of Region I, while for inset (b) the boundary has partially crossed the sphere and is needed to produce a convergent estimate of the heat flow. The Spitzer–Härm upper limit for $\epsilon \simeq 0.01$ is essentially between these two portraits. A similar outside to inside incursion is seen in the Grad closure pictures in Figure 8. As ϵ increases into the needed "finite" regimes of astrophysical problems, the Region I incursions of both closures further crowd the green circle at $\nu = \nu_\gamma$, eventually leading to the additional domain II incursions with negative $\mathbb{F}$ occurring inside $\nu_\gamma \simeq 2$. The misordering of this regime is now clear in both closures, since the presumed perturbative correction in Equation (1) has now grown to be able to compete and reverse the sign of the total unperturbed velocity distribution supporting closure inside two thermal speeds, while still doing this at suprathermal speeds because of the omnipresence of domain I effects. In this regime connection with the Boltzmann interpretation is nearly impossible. Hopefully Figures 7 and 8 help to convey that these are not an

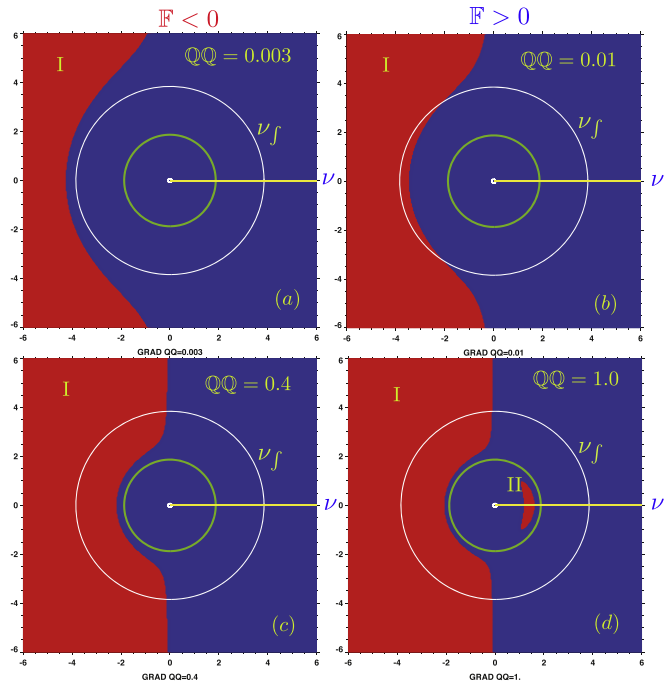

Figure 8. Grad 8 Moment progression of $\mathbb{F} < 0$ with increasing $\epsilon = \mathbb{QQ}$. Similar features and progression as seen in Figure 7.

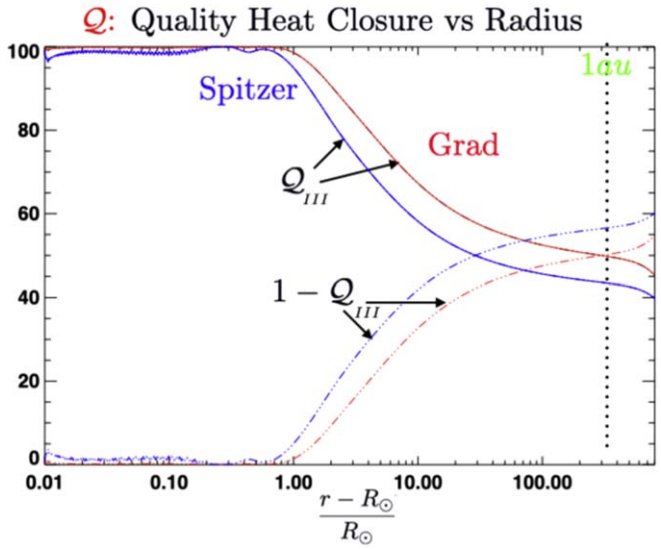

Figure 9. Spitzer Grad $\mathcal{Q}_{\rm III}(R)$ vs. R in a theoretical solar wind profile determined from the numerical wind profile reported by Cranmer et al. (2007). Nearly a 60% decrease in quality is recorded between the base of the corona and $10R_\odot$, precisely the region where the coronal temperature maximum is to be explained and the acceleration and asymptotic speed states of the wind are determined.

appropriate physical description for these plasmas with these Knudsen numbers.

8. Solar Wind Quality Variation versus Radius

In order to translate these findings to radial profiles, a well known numerical solar wind solution (Cranmer et al. 2007) has been used to estimate the radial variation of the electron temperature Knudsen number $\mathbb{K}_T$ and thus $\epsilon(r)$. This simulation invoked Spitzer's closure for the inner solar wind solution across the acceleration region and coronal temperature maximum before switching to another closure for larger distances. Here the published numerical profile is used to give profiles of the coordinated variation of n, T_e necessary to survey the regimes of $\mathbb{K}_T$ they suggest. Upon interpolating from Figure 6 for each $\epsilon(r)$ of the numerical solar wind solutions, the profile for $\mathcal{Q}_{\rm III}(r)$ in Figure 9 is produced.

Near 1 au Spitzer and Grad's heat closures have degraded 50%–60% from their high quality at the coronal base. Across the intervening domains the temperature maximum of the corona has formed and the dominant solar wind acceleration has occurred. This picture gives a graphical picture of the spatial decay of the quality of the kinetic transcription via the closure into the fluid modeling. Even across the radial domain where Spitzer's closure was retained the closure would appear to have decayed by the present quality measure by over 50%.

9. Discussion

An approach that gives a quantitative and visual portrait for the collapse of the perturbation expansion involving Spitzer-Braginksii and Grad closures has been presented. Based on the idea that physical closures having the highest quality should be based on substantially nonnegative closure velocity distributions, this approach uses the percentage contribution to the highest order moment from $\mathbb{F} < 0$ reported by the closure to quantify the closure's quality. The method is applicable to any closure approximation that specifies an underlying velocity distribution, rather than a stand alone postulate between fluid moments. In principal Landau fluid treatments Hammet & Perkins (1990) and Hunana et al. (2019a, 2019b) are open to such positivity analysis. This measure of quality involves comparing the approximate closure's moment with the restricted value for that moment from only nonnegative $\mathbb{F}$.

In this sense the quality check discussed here is one of internal consistency between the fluid level functional constraints of the closure studied, and the microscopic physical properties of $\mathbb{F}$ as a probability density. A different form of internal consistency is performed with Landau fluid models, by showing that they can recover the frequency dependent kinetic behavior expected from the Vlasov dispersion relation or from full nonlinear Vlasov solutions with full fluid models tailored to model the same initial conditions. In this sense the quality checks play the role of providing a "veto," since no closure that is internally inconsistent can be in the competition for the physically appropriate closure for the physical system under study. Using the Landau fluid closure as an example, its dispersion fidelity to Vlasov may be enforced with widespread unwanted negative total phase space density supporting the moments involved.

This paper has concentrated on the Spitzer-Braginskii and Grad 8 (SBG) closures to illustrate the method and also give a visual argument against modeling the solar wind with such inappropriate closures when the Knudsen number exceeds 0.01. The findings summarized next are specific to (SBG) closures, but the circumstances that permit their failure can recur in other closures under development (see Section 10).

Defining quality as the percentage of the closure's heat flux moment supported by nonnegative phase densities $\mathbb{F} > 0$, the known analytic regime for Spitzer–Braginskii convergence is shown to correspond to the first pitch angle averaged incursion of negative $\mathbb{F}$ into the sphere of radius ν_f, where it can numerically impact the third moment (heat flux) inventory. With growing expansion parameter, ϵ, analytical, graphical,

and numerical evidence (Figures 7 and 8 insets (a)–(d)) show that the unphysical phase space incursion of $\mathbb{F} < 0$ grows first at large speeds in phase space with pitch angles opposed to the heat flow, then is followed by a disjoint positive pitch angle region inside $\nu = \nu_\gamma \simeq 2$ that produces the increasing closure heat flow reported for $\epsilon > \simeq 0.7$. A very counterintuitive insight of these displays is that although $\mathbb{F} < 0$, the locales of their occurrence can continue to increase the positive heat flux along the magnetic field. In other words, the manifestation of negative $\mathbb{F}$ does not always present unphysically signed moment quantities; rather they are just unsupportable in their size or functional dependence on ϵ.

A model solar wind solution (Cranmer et al. 2007) has been used to illustrate the 50%–60% degradation of closure quality with heliocentric radius between the base of the corona and 1 au using the SBG closures. The solar wind's systematic growth of ϵ versus radius is arguably present around most stars (Scudder & Karimabadi 2013). Accordingly, similar degradations in SBG closure quality should also be expected in this type of astrophysical modeling.

The heat/energy inventory predicted by SBG closures in such regimes must surely be viewed with suspicion; agreements or disagreements between fluid models with SBG closures and observables (when $K > 0.01$) can have no ready implication about the physical incompleteness of the description of the system modeled.

Conversely, modifying the fluid scale physics modeling to include additional processes to improve agreement with data in the presence of such SBG closures cannot be used to infer the need for these new fluid scale processes: a logical possibility of such an approach is that the posited new physics incorporated has inferred properties that compensate for the quality inadequacies of the SBG closures still being used.

In addition, such a modeling strategy is retaining a broken closure formalism for what is hoped to be the improved physical model of the corona solar wind expansion. The most secure argument for new physical processes to explain coronae and stellar winds are produced when the new effects are demonstrated to play the postulated role when (i) accomplished with closures shown a posteriori to be consistent that (ii) also describe all baseline competitive mechanisms in a consistent way. Demonstrating the need for hydromagnetic damping to explain the observed coronal–solar wind properties is clearly not consistently done with a broken SBG closure, supplying a demonstrably defective heat flux. In such an attempt SBG is being exploited for its pro forma, but invalid, closure that mathematically allows a fluid model containing new physical effects to be constructed. Using SBG in such a demonstration ensures that heat conduction's role is not allowed to compete for the explanation, but artificially does ensure there is a finite, but inconsistent, list of partial differential equations to solve when modeling hypothetical processes in the corona and solar wind. This is unethical.

10. Closure Horizons

This paper closes with a brief survey of other approaches for modeling large-scale astrophysical plasmas that attempt to solve approximate versions of the problem rather than the entire kinetic one. The spirit of this survey is to identify briefly what alternatives to SBG are available, and of these are there some that are, or are not, plagued with the same types of liabilities shown above to have been detrimental to SBG closures.

The SBG analysis of this paper has demonstrated that unphysically negative probability distribution functions dominate the heat flux reported by the closure when used for $K > 0.01$. The large variations of K seen in astrophysical plasmas are caused both by decreasing densities and temperatures (collisionalities), but also by steep gradients imposed on these systems by external forces of gravity, rotation, and radiation.

(i) Exospheric approaches model large plasma volumes and their pervading spatially dependent forces as if the medium had no collisions or wave-particle interactions; they obtain solutions of the Vlasov equation with pervasive $\mathbb{F} \geqslant 0$, guaranteed (Lemaire & Scherer 1973). The solutions are determined by the assumed boundary conditions that require specification of the velocity distribution assumed there.

Modern versions of such solutions can produce solar wind solutions with a wide range of asymptotic speeds, which SBG cannot do with its broken heat recipe. Different classes of solutions have been exhibited as a function of the phase space boundary conditions assumed for Vlasov; when the boundary VDFs are supposed to be nonthermal (Scudder 1992) the entire observed spectrum of solar wind speed states are produced by the underlying exospheric approach (Zouganelis et al. 2004).

As usually performed, this approach incorporates variable magnetic, gravitational, rotational, and parallel electric fields that are smooth on the ion gyro scale, but are not restricted in gradient scales beyond this. In the usual sense of closures this approach and its results are nonperturbative.

Three other approaches that guarantee $\mathbb{F} \geqslant 0$ include (i) coulomb collisions while neglecting wave-particle effects, (ii) sizable $E_\parallel$, and (iii) the force of gravity, which are all known to be present in this class of astrophysical system:

(ii) The Fokker–Planck analytic-numerical approach was used to improved the suprathermal heat flow description, including collisions, but retained no wave-particle interactions (Olbert 1983). The progress demonstrated by this approach used a semi-empirical form of the scaling of $E_\parallel$, explicitly generating transonic wind solutions compatible with the strong parallel electric field. Not only did this approach generate high speed winds, it also produced the nonmonotonic proton temperature profile. Since a version of the kinetic equation was solved, $\mathbb{F} \geqslant 0$ was guaranteed. The method is not perturbative.

(iii) A scaled Monte Carlo model has also been developed to recover the solar wind expansion, while explicitly incorporating speed dependent Coulomb collisions, but without incorporating wave-particle processes (Landi et al. 2012). This approach determines self-consistently the size of $E_\parallel(s)$ and agrees that it is large, with $\mathbb{F} \geqslant 0$ computed as a probability. These models have recovered the observed ubiquitous nonthermal form of the electron VDF, without assuming wave-particle effects. The authors suggest that the fidelity achieved with such a simple model demonstrates the essential role of coulomb collisions in the wind formation, already suggested earlier. By construction this method excludes wave-particle interactions and iterates to find a steady-state (Neugebauer 1976; Scudder & Olbert 1979). The method is not perturbative and determines $E_\parallel$ self-consistently; it is large and comparable to its size estimated by other methods.

(iv) SERM is a new approach under development (Scudder 2019b). It is predicated on getting a much better lowest-order distribution function from which to seek the transport description. Arguably $\mathbb{F}^o_{\rm SERM}$ is much closer to the description of the distribution function observed than any of the methods described. Regardless of the size of $E_\parallel$, $\mathbb{F}^o_{\rm SERM} \geqslant 0$ and is generally kurtotic, but reduces to a Maxwellian when $E_\parallel = 0$. The substantial size of $E_\parallel(s)$ known empirically to characterize the solar wind is respected in this approach at nearly every consideration. The radial profile of $E_\parallel(r)$ needed is determined self-consistently. The approach is nonperturbative and nonnegativity of $\mathbb{F}$ occurs by construction.

(v) The fifth approach is usually referred to as Landau (Fluid) closures (Hammet & Perkins 1990; Snyder et al. 1997; Josefs & Dimits 2016; Hunana et al. 2019a, 2019b). These started as methods to describe with fluid variables how a truly collisionless Vlasov plasma would behave. Because these fluid equations represent moments of the Vlasov kinetic equation (and sometimes a collision operator), aspects of wave-particle interactions and particle collision competitions can be addressed, but at the fluid level, rather than performing Boltzmann simulations. Of particular importance in the Landau approach is the incidence of resonance described at this level and a particular approach to truncating the fluid equations for this type of description (than can in principle be done at an infinite number of places) but are usually imposed on the first moment above the heat flux.

The frequency and wavenumber dependence of the tensorial elements of the fourth moment's tensor are adjusted to maximally improve the agreement between the Landau Fluid simulation and Vlasov dispersion relation. Usually the agreement cannot be made perfectly, and often is performed for a given mode of particular interest (of those allowed) by matching behavior $\omega \downarrow 0$ and $\omega^{-1} \downarrow 0$ as predicted by the dispersion relation from the linearized Vlasov equation. The truncation recipe makes the Landau Fluid response appear as if modified by phase mixing, and Landau damping, which of course helps to destroy actual resonances and produce answers rather than divergences, while also allowing predictions from the fluid model possible for non-resonant $k - \omega$ pairs. This procedure produces a delocalized description for the heat flows associated with specific modes.

A key part of the theory is that the dispersion relation problem for the linearized Vlasov system must be solved before its properties can be imposed on the closure choices of the Fourier transform of the tensors contained in the fourth moment. The zeroth-order initial plasma state must be in equilibrium before computing a dispersion relation. This consideration is the origin of the limitations in the Landau literature that the systems where it can be used must not contain zeroth-order forces along the magnetic field. In particular, consideration of the evolution of perturbations in the presence of lowest-order accelerations along the local magnetic field are outside the scope of Landau Fluid closures presently known to this author. This impediment is particularly germane for astrophysics with its ubiquitous lowest-order and prominent $E^o_\parallel$, caused by gravity.

The Landau Fluid closure is a perturbative approach; it imposes an internal check that the plasma reaction in the fluid model is truly reflective of the Vlasov dispersion relation. However, still being perturbative there remains the question of whether the fluid model's finite order prediction of the total velocity probability distribution remains nonnegative. In this sense the mathematically elegant Landau Fluid closure does not preclude its fluid theory being based on underlying $\mathbb{F} < 0$. This is the same possibility that caused perturbative SBG($K > 0.01$) to fail.

The present inability to perform linearized dispersion analysis with lowest-order $E_{\parallel,o}$ restricts the class of problems that can use this approach. Also unclear is how a Landau Fluid closure tailored to describe Mode A behaves when the system develops multiple modes either nonlinearly or from initial value preparation.

This brief overlook shows that:

I. Some, but not all, approaches ensure that their solutions automatically satisfy $\mathbb{F} \geqslant 0$; the possibility of violations of that condition was a prominent signature for the collapse of SBG shown above.
II. Multiple approaches preclude wave-particle effects, but have claimed that speed dependent coulomb collisions are central to their success describing the observed solar wind's behavior.
III. Multiple approaches permit nonzero steady-state parallel electric fields $E^o_\parallel$; such fields in astrophysical plasmas are omnipresent caused by gravity and rotation and observed in the solar wind steady state.
IV. Some approaches as developed in the literature restrict their suitability to systems where equilibrium field aligned forces are not allowed.
V. Multiple approaches in group I were demonstrated to have the $\mathbb{F} \geqslant 0$ property regardless of inclusion of coulomb collisions, specific wave-particle effects, or degree of collisionality presumed.
VI. Several approaches that argue that coulomb collisions are pivotal for the wind's description even reproduce the observed velocity space distributions of the electrons, not just their overall moment behavior and support of the observed wind.
VII. Several perturbative approaches retain the liability, like that shown in the SBG closures, that the approximate fluid solutions might be predicated on unphysical $\mathbb{F} < 0$ velocity probability distributions.

There are multiple alternate paths open for exploration and modeling improvement that do not insist on using SBG closures. Of those listed there are commonalities and differences that distinguish the different approaches surveyed. The liabilities of a given approach would appear to increase with (i) the possibility of $\mathbb{F} < 0$ occurring in the theoretical approach, (ii) the inability of the method to address the now well known parallel forces, like $E^o_\parallel$, in astrophysical plasmas, or (iii) stipulation that omnipresent collisions are not present.

Digital data from the solar wind solution provided by Cranmer et al. (2007) has been reorganized as described in the text for use in Figure 9. The author has profited from exchanges with the editor and referees. This paper's research was partially supported by NASA grant 80NSSC19K1114.

Appendix

This appendix outlines the speed domains that determine the size of the improper moment integral for the heat flux. When fully expanded Equation (11) is in the form of a sum of three

separate integrals for which the identity

$$\exp(-\nu^2)\nu^n \equiv \exp(-\nu^2 + n \cdot \ln \nu) \tag{20}$$

yields a very good, but different, approximation for each integral, by modifying the integrands using:

$$\exp(-\nu^2)\nu^n \simeq \exp(-\nu_*^2)\nu_*^n \exp(-2(\nu - \nu_*)^2); \tag{21}$$

the peak of this approximate form of Equation (20) occurs at

$$\nu_*(n) = \sqrt{\frac{n}{2}}. \tag{22}$$

The second derivative of the Taylor series evaluated at the peak of the second exponent in Equation (20) is -4, implying a second-order accurate approximate form for Equation (20) is

$$\exp(-\nu^2)\nu^n \simeq A^*(\nu_*)\exp\left[\frac{-(\nu - \nu_*(n))^2}{2\left(\frac{1}{2}\right)^2}\right]$$
$$A^* = \exp(-\nu_*^2)\nu_*^n, \tag{23}$$

a displaced Gaussian, centered on ν_* given by Equation (22) with half width in ν of $1/2$. To estimate this contribution to the moment requires tabulation about its peak across the ν interval

$$|\nu - \nu_*(n)| \leqslant \frac{3}{2}, \tag{24}$$

corresponding to the contributions ± 3 half widths of the three equivalent Gaussian model peaks.

The integrals for the heat flux involve speed exponents $n = \{11, 9, 5\}$ for Spitzer and $n = \{10, 8, 5\}$ for Grad's closures. Thus numerical integration requires the tabulation and properties of $\mathbb{F}(\nu, \mu)$ between

$$0.08 \simeq \sqrt{\frac{5}{2}} - \frac{3}{2} \leqslant \nu_S \leqslant \sqrt{\frac{11}{2}} + \frac{3}{2} \simeq 3.85 \tag{25}$$

for Spitzer, and between

$$0.08 \simeq \sqrt{5/2} - \frac{3}{2} \leqslant \nu_G \leqslant \sqrt{5} + \frac{3}{2} \simeq 3.74 \tag{26}$$

for Grad. Summarizing, the moments including the heat flow require tabulation at least across the interval

$$0.08 \leqslant \nu \leqslant 3.85 \text{ speed/w interval}$$
$$0.0064 \leqslant \frac{E}{kT} \leqslant 14.8 \text{ energy}/kT \text{ interval} \tag{27}$$

that spans a range in the probability distribution function of $1 \leqslant f(\nu) \leqslant 3.6 \times 10^{-7}$.

ORCID iDs

J. D. Scudder https://orcid.org/0000-0001-7975-5630

References

Chandran, B., Dennis, T., Quaetert, E., & Bale, S. D. 2011, ApJ, 743, 197C
Cranmer, S. R., van Ballegooijen, A. A., & Edgar, R. J. 2007, ApJS, 171, 520
Gombosi, T. I., van der Holst, B., Manchester, W. B., IV, & Sokolov, I. V. 2018, LRSP, 18, 4
Grad, H. 1949, CPAM, 2, 331
Gray, D. R., & Kilkenny, J. D. 1980, PlPh, 22, 81
Gurevitch, A. V., & Isotomin, Y. N. 1979, JETP, 50, 470
Hammet, G., & Perkins, F. 1990, PhRvL, 64, 3019
Hazeltine, R. D., & Waelbroeck, M. L. 1998, The Framework of Plasma Physics (Boulder, CO: Perseus Books)
Hunana, P., Tenerani, A., Zank, G. P., et al. 2019a, JPlPh, 85, 205850602
Hunana, P., Tenerani, A., Zank, G. P., et al. 2019b, JPlPh, 85, 205850603
Josefs, I., & Dimits, A. M. 2016, CoPP, 56, 504
Killie, M. A., Janse, A. M., Lie-Svensen, O., & Leer, E. 2004, ApJ, 604, 842
Landi, S., Matteini, L., & Pantellini, F. 2012, ApJ, 760, 143
Lemaire, J., & Scherer, M. 1973, RvGSP, 11, 427
Levermore, C. D. 1996, JSP, 83, 1021
Manchester, W. B., IV, van der Holst, B., Tóth, G., & Gombosi, T. I. 2012, ApJ, 756, 81
Matsumoto, T. 2021, MNRAS, 500, 4779
Neugebauer, M. 1976, JGR, 81, 78
Ng, J., Hakim, X., & Bhatacharjee, A. 2018, PhPl, 25, 082113
Olbert, S. 1983, JPL Solar Wind 5 NASCP2, 880, 149
Reville, V., Tenerani, A., & Velli, M. 2018, ApJ, 866, 38
Schiff, A. J. 2020, PhD thesis, Univ. Colorado, Boulder CU, 5/2020, ProQuest 27958933
Schoub, E. C. 1983, ApJ, 266, 339
Schunk, R. W. 1977, RGSP, 15, 429
Scudder, J. D. 1992, ApJ, 398, 319
Scudder, J. D. 2019a, ApJ, 885, 148
Scudder, J. D. 2019b, ApJ, 885, 138
Scudder, J. D., & Karimabadi, H. 2013, ApJ, 770, 26
Scudder, J. D., & Olbert, S. 1979, JGR, 84, 2755
Scudder, J. D., & Olbert, S. 1983, in JPL Solar Wind Five, ed. M. Neugebauer (Washington, DC: NASA), 163
Snyder, P. B., Hammet, G. W., & Dorland, W. 1997, PhPl, 4, 3974
Spitzer, L. J., & Härm, R. 1953, PhRv, 89, 997
Struchtrup, H. 2005, Macroscopic Transport Equations for Rarefied Gas Flows (Heidelberg: Springer)
Usmanov, A. V., & Goldstein, M. 2006, JGRA, 111, A07101
van der Holst, B., Manchester, W. B., IV, Franzin, R. A., et al. 2010, ApJ, 725, 1373
van der Holst, B., Sokolov, I. V., Meng, X., et al. 2014, ApJ, 728, 81
Zouganelis, I., Maksimovic, M., Meyere-Vernet, N., Lemy, H., & Issautier, K. 2004, ApJ, 606, 542